# Investigation of the Negative Thermal Expansion Mechanism of Zeolite Chabazite Using the Pair Distribution Function Method

**María M. Martínez-Iñesta*,† and Raúl F. Lobo*,‡**

*Center for Catalytic Science and Technology, Department of Chemical Engineering, University of Delaware, Newark, Delaware 19716*

*Received: December 22, 2004; In Final Form: March 21, 2005*

We have used the pair distribution function (PDF) method to gain insight into the mechanism of contraction of zeolite chabazite. Using this method we followed how the interatomic distances of the local structure changed with temperature. By optimization of the structure by free energy minimization and using the Reverse Monte Carlo technique we were able to find structural models at low and at high temperatures that agreed quantitatively with our experimental PDFs. From these models we conclude that the mechanism of contraction with temperature cannot involve rocking of the tetrahedra as rigid unit modes as there are distortions of the tetrahedra with temperature (indicating internal vibrations) and also that the mechanism of contraction probably involves a mode that translates along the Si−O3−Si−O4−Si linkages inside of the D6R of zeolite chabazite.

## Introduction

Most materials expand with temperature because the effective bond distance between atoms increases with temperature. However, recently many oxides have been found to contract with temperature, that is, they exhibit a negative thermal expansion (NTE) coefficient. Many zeolites have been found to have this property and variable-temperature studies using neutron and X-ray powder diffraction and microcrystal X-ray diffraction have shown that siliceous zeolites with framework structures MWW,[1] ITE,[1] STT,[1] MFI,[2] AFI,[2] DOH,[2] MTN,[2] DDR,[2] ISV,[3] STF,[3] IFR,[4] and CHA,[4] among others, all show NTE at some temperature range. The evidence shows that in zeolites negative thermal expansion is becoming a rule rather than an exception.

Chabazite (CHA) (see Figure 1) is particularly interesting as it has the largest NTE coefficient known in aluminosilicates, a maximum of $-16.7 \times 10^{-6}$ $K^{-1}$ over the temperature range 293−873 K (ALPO-17 has the largest known coefficient of negative thermal expansion of any material[5]), as was shown by Woodcock et al. using powder neutron diffraction.[4] The mechanism for this phenomenon has been explained in terms of the presence of rigid unit modes (RUMS) in zeolites,[6] that is, modes in which the Si−O distances and O−Si−O angles of the tetrahedra stay nearly constant with temperature, acting as a rigid unit but with a rocking mode between units that causes the contraction. These RUMS are present in many zeolites due to the flexibility of their framework and their presence and directions can be calculated using the program CRUSH developed by Hammonds et al.[7] Nevertheless, Tao and Sleight[8] have found that the presence of RUMS does not necessarily predict negative thermal expansion in oxide structures and vice versa. This suggests that the mechanism of NTE should not be assigned automatically to RUMS and that the mechanism may be different for different structures.

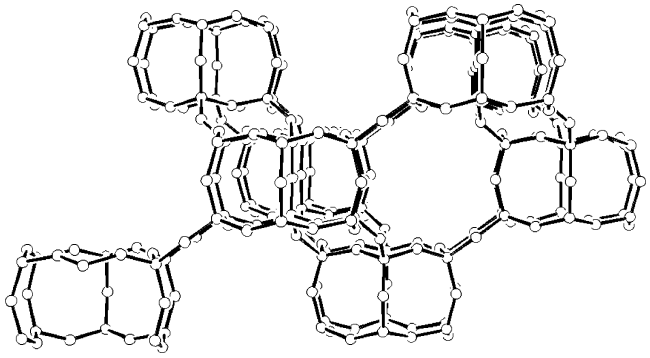

**Figure 1.** View of a double six membered ring (D6R) of chabazite down the a axis. Each ring is made up of alternating Si−O1−Si−O3 bonds connected to the other ring via Si−O4−Si bonds. Each D6R then is connected to another D6R via Si−O3−Si−O2 bonds.

There is another structural characteristic of zeolites that can be observed as a consequence of the stress that cations put on the framework: they can be collapsible or noncollapsible.[9] Collapsible frameworks are those in which the Si−O−Si angles become as low as possible or one in which the framework completely coordinates the occluded cations. In noncollapsible frameworks usually two adjacent Si−O−Si angles antirotate. This behavior might correlate well with the behavior of zeolites under thermal stress and might give an insight into a possible contraction mechanism.

Knowledge of how zeolites behave as a function of temperature is important as they are used in practice as catalysts at high temperature and the dynamics of the structure can affect the reaction mechanisms and the transport of molecules within the pores. In addition the negative thermal expansion can be an opportunity to new commercial applications as thermal stress resistant materials. If used in a composite material, for example, you can ideally achieve a zero or specific value expansion material under certain conditions. Possible applications for these materials would be in high precision optics, where the optical properties do not degrade with temperature, ceramics, for

* Address correspondence to these authors.
† E-mail: martinm@che.udel.edu.
‡ E-mail: lobo@che.udel.edu.

10.1021/jp044165w CCC: $30.25 
Published on Web 04/23/2005

resistance to thermal shock, dental fillings, where its expansion is matched to the teeth, etc.[10]

In this paper we use the pair distribution function (PDF) technique as a complementary approach to gain more insight into the mechanism of contraction of chabazite with temperature. We have shown that this technique can be used to determine the local structure of complex disordered zeolites such as beta[11] and here we use it to investigate the evolution of the local structure of siliceous chabazite at different temperatures. Using the PDF we will be able to look at how the interatomic distances change with temperature and we will be able to discern between possible NTE mechanisms. One of the advantages of using the PDF method is that in addition to the Bragg periodic information it also uses the diffuse disorder information of the structure. Details about the pair distribution function are readily available[12−14] but here we give the essential elements to understand the methodology.

The pair distribution function $G(r)$ is the distribution of density of interatomic distances in a material that can be obtained either from high-energy X-ray or neutron diffraction data. The relation is described as:

$$G(r) = 4\pi r(\rho(r) - \rho_o) = \frac{2}{\pi}\int_{Q_{min}}^{Q_{max}} Q[S(Q) - 1]\sin(Qr)\,dQ \quad (1)$$

where $r$ is the interatomic distance, $\rho(r)$ is the microscopic pair density, $\rho_o$ is the average atomic density of the material, $Q = 4\pi \sin(\theta)/\lambda$ is the scattering vector, and $S(Q)$ is the corrected and normalized scattering data. The integration must be done to high $Q$ to minimize termination errors that come from cutting the integration short, thus the need for a high-energy radiation source.

One important difference between a regular diffraction study and a pair distribution function study is that in a diffraction structural study only the Bragg peaks scattered by the average crystalline structure are used and in a pair distribution function study both the sharp Bragg peaks and the broad diffuse peaks scattered by the atoms deviating from the average structure are used. Only the incoherent Compton scattering is removed from the scattering data, as it does not contain structural information.

The experimental PDF can be calculated from a structural model by using the equation:

$$G(r) = \frac{1}{r}\sum_{i,j}\frac{b_i b_j}{\langle b\rangle^2}\delta(r - r_{ij}) - 4\pi r\rho_o \quad (2)$$

where the sum is over all atoms in the sample, $r_{ij}$ is the distance between atoms $i$ and $j$, $b_i$ is the scattering length of atom $i$, and $\langle b\rangle$ is the average scattering length of the sample. The scattering lengths using X-rays are the form factors and are usually assumed constant at a specific value of $Q$.

To be able to study the structural changes of zeolite chabazite with temperature we need a structural model that describes well the experimental PDFs at different temperatures. We have found that the structures obtained by Woodcock et al.[4] did not describe well the actual local structure of chabazite at high temperatures.

Tschaufeser and Parker[15] and Gale[16] have demonstrated that free energy minimization of the structures of zeolites using zero static internal stress approximation (zsisa) is suitable for the investigation of the thermal expansion of zeolites. Using this approximation the internal variables of the structure are minimized with respect to the internal energy while only the strain variables are minimized with respect to the free energy. One of the successes of lattice dynamics in this area was the prediction of negative thermal expansion of certain framework materials, which was subsequently verified experimentally.[17] We have, thus, used this method within the program GULP[18] to obtain an initial model of the structure of chabazite at the experimental temperatures.

Using this structural optimization method and Reverse Monte Carlo we were able to find a structural model that agreed quantitatively with the experimental PDFs of chabazite at low and high temperatures. We were able to determine the static structural changes of chabazite with temperature and prove that the mechanism of contraction of chabazite is not rigid rocking of the tetrahedra.

## Experimental Methods

**Synthesis.** Siliceous chabazite was synthesized following a procedure similar to that reported by Díaz-Cabañas et al.[19] using *N*,*N*,*N*-trimethyladamantammonium ($TMAda^+$) as structure directing agent.

The reaction mixture had a composition of $0.024Si(OC_2H_5)_4$: $0.12TMAda{:}0.012HF{:}0.08H_2O$, where $Si(OC_2H_5)_4$ is tetraethyl orthosilicate (TEOS; Aldrich, 98%).

The structure directing agent in the hydroxide form (TMAdaOH) was synthesized by mixing 40 g of 1-adamantammonium (Aldrich, 97%) with 200 mL of *N*,*N*-trimethylformamide (Aldrich, 99%) and 150 mL of tributlyamine (Aldrich, 99%). The solution was stirred in an ice bath until the 1-adamantammonium dissolved. $CH_3I$ (50 mL; Aldrich, 99.5%) was then added dropwise. The mixture was allowed to mix for 2 h in the ice bath after which the beaker containing the solution was covered with Parafilm and tin foil and allowed to react statically for 4 days. The solution was then filtered and washed with acetone until the resulting TMAdaI powder was white. The SDA was ion exchanged into the hydroxide form by mixing 13 g of TMAdaI with 30 mL of deionized water and 155 mL of a basic ion-exchange resin (J. T. Baker, Na-38, $^-OH$ form). After 2 days the resin was filtered and washed with deionized water and the resulting TMAdaOH solution was collected. The SDA solution was titrated with aqueous 0.0979 M HCl (Aldrich, originally 0.979 M) and was found to have a concentration of 0.25 M. The solution was then placed in a Rotovap and water was removed until the concentration reached approximately 0.78 M.

The all-silica chabazite was synthesized by mixing 5.04 g of TEOS with 15.3 mL of the 0.78 M template solution. The mixture was placed on a heating mantle to evaporate all of the ethanol and 93% of the water resulting in a total weight loss of 16.43 g. The evaporation was carried out slowly over a long period of time. Next, 0.48 g of an aqueous hydrofluoric acid solution (Merck, 47−51 wt %) was added. The mixture was stirred until homogeneous and then placed in 20-mL Teflon-lined Parr autoclaves. The mixture was heated under rotation of 60 rpm at 150 °C for 38 h. The synthesis product was then filtered and washed with deionized water. The chabazite sample was calcined in air by heating the sample at 1 deg/min to 50 °C and then left at this temperature for 1 h. The sample was then heated 1 deg/min up to 580 °C and held at this temperature for 6 h.

**Analytical Measurements.** In-house X-ray powder diffraction (XRD) patterns were obtained on a Philips X'Pert diffractometer using Cu Kα radiation. The patterns were collected from 1° to 50° in 0.02° steps with 1.75 s per step. The pattern was indexed and the unit cell parameters refined. The refined values of the unit cell parameters in the hexagonal $R\bar{3}m$ space group are $a = b = 13.511(6)$ Å and $c = 14.709(2)$ Å.

The MAS NMR spectra were recorded on a Bruker MSL 300 MHz spectrometer ($B_o = 7.4$ T) operating at resonance frequencies of 59.627 MHz. The $^{29}$Si MAS NMR spectra were obtained in 7 mm rotors at a spinning rate of 3 kHz. 3-(Trimethylsilyl)-1-propanesulfonic acid (DSS) was used as the chemical shift reference. A $\pi/3$ pulse of 4 $\mu$s was used with a recycle delay of 30 s between each scan. $^{29}$Si{$^1$H} CP NMR spectra were obtained. A $^1$H $\pi/2$ pulse and $^{29}$Si $\pi/4$ pulse were set to 6 $\mu$s and 4 $\mu$s, respectively, with a contact time of 3 ms.

**Optimization of Framework Structures.** The structures of chabazite at 293 and 873 K from Woodcock[4] were optimized with GULP, using the force field model and parameters reported by Gale.[16] Catlow's zeolite force field library included in GULP and Burchart's zeolite force field included in Cerius[2] were also used to optimize the structure but Gale's model was found to be a better fit to the experimental PDF. All minimizations were conducted without any soft constraints using the original space group, hexagonal $R\bar{3}m$. We also minimized the free energy of the structures using GULP with and without the zero static internal stress approximation at 308 and 753 K.

**Synchrotron Data Acquisition.** The data for the X-ray pair distribution function was obtained at the SRI-CAT 1-ID beam line at the Advanced Photon Source, Argonne National Laboratory. The measurements were conducted in symmetric transmission geometry at 308 and 753 K. A Si (111) crystal monochromator was used to obtain incoming X-rays with 80.7 keV energy ($\lambda = 0.1537$ Å). The diffracted photons were collected with an intrinsic germanium detector connected to a multichannel analyzer. Several diffraction runs were conducted with the sample at room temperature and the intensities were averaged to get better statistics. Each run was divided in two sets: from $2\theta = 0.8°$ to 5.8° the scan was measured with a step size of 0.01° with 5 s per step and from 5.8° to 78° the scattering was measured with a 0.02° step size of 3 s per step. The averaged data were normalized for flux, corrected for detector dead time, background, Compton scattering, and absorption, and then converted to total scattering structure factor, $S(Q)$.[20,21] The structure factor was cut at $Q = 20$ Å$^{-1}$ to minimize the Fourier transformation of statistical noise in the data at high $Q$ into real space. The data treatment was done with the program PDFgetX.[22]

**Real-Space Rietveld Refinement of the Structure.** The procedure followed was described before[11] and will only be summarized here. Two types of refinements were done on the structures depending on the purpose. The first type was mainly a PDF profile refinement in which we changed the parameters that are affected by the data treatment, the instrument, and the structural details particular to PDF. These parameters are the scale, instrumental resolution, displacement parameters, and a parameter called *delta* reflecting the correlation of the motion of neighboring atoms. It is relevant to point out that studies using the PDF method have found that only limited information of the correlation of atoms can be extracted from the data. Jeong et al. have found that a simple model describes the effects of lattice vibrations on the PDF peak widths.[23] In PDFfit[24] delta simulates this correlation of the motion of atoms by sharpening the peaks at lower $r$ and cannot be obtained with any other crystallographic method. We used the same atomic displacement parameters for both types of atoms because the refinement had a tendency to give larger numbers for the silicon atoms than for the oxygen atoms when it is known that this is not the case. We did not use the experimental displacement parameters found by Woodcock et al.[4] because of their lack of physical significance (negative isotropic displacement parameters for the oxygen atoms). It is interesting, however, that they also found that the displacement parameters of the oxygen atoms were consistently lower than those of the silicon atoms. We did not obtain experimental displacement parameters with our scattering data because the resolution necessary for our PDF analysis is lower than is needed for a Rietveld refinement. This initial profile refinement was conducted to assess the agreement of the structure with experiment as none of the structural parameters were changed.

The second type of refinement started with the refinement of the lattice cell parameters. Then the profile parameters were refined followed by the atomic positions. We refined the structures in their rhombohedral setting using the form factors at $k = 0.8$ Å$^{-1}$. The goodness of fit parameter of the PDF refined models is given by:

$$R_w = \sqrt{\frac{\sum_{i=1}^{N} w(r_i)[G_{obs}(r_i) - G_{calc}(r_i)]^2}{\sum_{i=1}^{N} w(r_i) G_{obs}{}^2(r_i)}} \tag{3}$$

**Combination of Reverse Monte Carlo Refinement and Real-Space Rietveld Refinement.** A combination of Reverse Monte Carlo refinement and real-space Rietveld refinement was done to the two optimized structures using DISCUS and PDFfit, respectively. In the Reverse Monte Carlo technique an atom in the structure is randomly selected and randomly moved in a random direction. The pair distribution function is recalculated for the generated move and the goodness of fit parameter $\chi^2$ is computed:

$$\chi^2 = \sum_{i=1}^{N} \frac{[I_e(r_i) - I_c(r_i)]}{\sigma^2}{}^2 \tag{4}$$

where $I_e$ stands for the experimental intensity at point $r_i$ and $I_c$ stands for the calculated intensity. The change in goodness of fit is given by $\Delta\chi^2 = \chi_{old}{}^2 - \chi_{new}{}^2$. Every move that improves the fit to the data is accepted. Those moves that worsen the fit are accepted with a probability $P = \exp(-\Delta\chi^2/2)$. How many "bad" moves are accepted depends on the value of $\sigma$ that is treated as a parameter in DISCUS. To avoid structures that are either physically or chemically improbable we set a minimum distance for the Si−O, O−O, and Si−Si atomic distances. Also, the displacement was set to be a fraction of 0.002 of each unit cell parameter. This technique was used to obtain a chemically sensible disordered structure that would better describe the experimental PDFs. We expected a disordered structure to be a better fit to the experimental PDF because of the fact that the PDF also includes structural information from the diffuse scattering.

The real-space Rietveld refinement was conducted to obtain profile parameters that were adequate for each Reverse Monte Carlo refined structure. The procedure was first to refine the profile parameters of the optimized structure in PDFfit and then use those parameters to refine the structure with Reverse Monte Carlo. We used the rhombohedral setting for these refinements and the Reverse Monte Carlo was ran 10 000 cycles every time, using the information of the experimental PDF up to 18 Å. Once the structure was refined then the profile parameters were refined in PDFfit and the cycle was repeated until no change in the goodness of fit was observed.

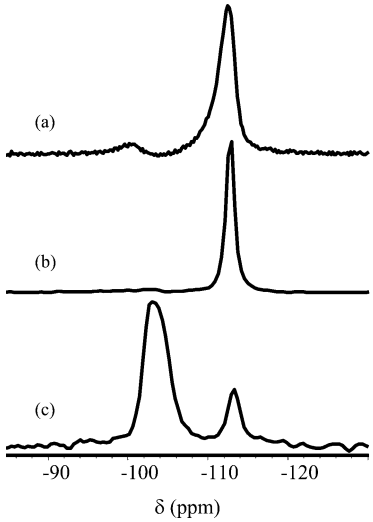


**Figure 2.** $^{29}$Si MAS NMR spectra of chabazite (a) as-made, (b) calcined, and (c) $^{29}$Si{$^{1}$H} CP MAS NMR (calcined).

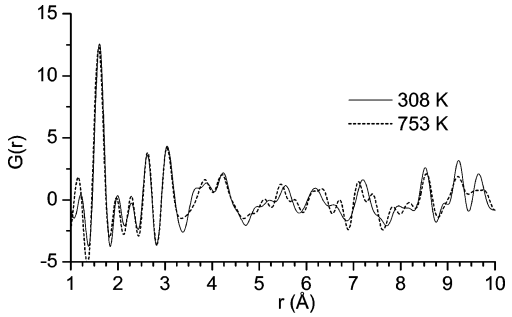


**Figure 3.** Two experimental PDFs.

## Results and Discussion

Results from powder XRD and NMR spectroscopy showed that we had a sample of highly siliceous pure chabazite. The $^{29}$Si MAS NMR spectra for the as-made material and calcined material are shown in Figure 2. The spectrum of the calcined material shows one sharp peak at −112.9 ppm corresponding to a silicon atom surrounded by four (−OSi) units. A very small peak is seen at approximately −102 ppm, which corresponds to the defect groups $(Si(OSi)_3)OH$ in the material. The relative peak intensities were used to calculate the approximate unit cell composition as $[Si_{36}O_{70.8}(OH)_{2.4}]$. This is close to that obtained by Diaz-Cabanas et al. ($[Si_{36}O_{70.5}(OH)_{2.9}]$).[19] As expected, the CP MAS spectrum (Figure 2c) shows an enhancement of the signal corresponding to the defect sites as these silicon atoms are closer in proximity to the hydrogen atoms.

The experimental PDFs obtained at $T_1 = 308$ K and $T_2 = 753$ K are shown in Figure 3. Comparison of the PDFs at the two temperatures shows that they share almost identical peaks at low and high $r$ distances while the peaks in the middle are only qualitatively similar. This reveals that the difference in the structure of chabazite at the two temperatures is more than simply a change of lattice parameters, which will only cause the peaks to be shifted, or more than a change in the Debye−Waller factor, which will cause all the peaks to be broadened. The fact that the peaks at low and high $r$ are similar, though, suggests that the structural changes with temperature are not simple.

The first two peaks are characterictic of the $SiO_4$ tetrahedra in zeolites. The peak at approximately 1.6 Å corresponds to the Si−O nearest distances, the second peak at approximately 2.62 Å corresponds to the O−O distances and the third peak at approximately 3.04 Å corresponds to the Si−Si distances. The two small peaks between the Si−O and O−O peaks are termination ripples caused by our limited $Q_{max}$ in the Fourier transform. It is clear from this figure that the average nearest Si−O distances, O−O distances stay approximately the same with the temperature increase. A fitting of a Gaussian curve to these peaks reveals that the Si−O average distance changes from 1.5958 ± 0.0003 Å to 1.5978 ± 0.0009 Å, which is negligible, and the O−O average distance increases from 2.610 ± 0.001 Å to 2.629 ± 0.005 Å. This might suggest that at 753 K the stretching modes between bonded atoms do not change from those at 308 K. Although the change in average O−O distances is appreciable, if it is considered that the $\Delta T = 445$ K the tetrahedra, on average, are not changing significantly and, thus, these results can be considered consistent with the theory that RUMs cause the NTE.

However, we can also see that the Si−Si peak is essentially the same and it is not until we get to the higher $r$ peaks that we observe any major difference. A Gaussian fit to this peak shows that the Si−Si peak changes from 3.0508 ± 0.0002 Å to 3.0438 ± 0.0002 Å, a decrease of less than 0.01 Å. At first glance this observation does not agree with the hypothesis that the NTE is caused by rocking of the tetrahedra as, if this were the case, we would expect the Si−Si peak to change due to the change in Si−O−Si angles. If there is in fact a rocking mode, it does not change with temperature and thus cannot cause the NTE.

The PDFs start to differ after 3.28 Å. The next two peaks correspond mainly to third and fifth neighbor Si−O distances, with the one at 4.25 Å having contributions from Si−Si distances. It is interesting to note that the peaks between 3.28 and 4.05 Å differ greatly while the peak at 4.25 Å remains nearly identical. This suggests that there is a very specific contracting mechanism in chabazite that involves the change of some specific Si−O distances. Based on these experimental observations a viable mechanism would involve twisting, or rotation, along the Si−O bonds of the tetrahedra acting as rigid units. This would explain the constant Si−Si average distance and the change in the rest of the structure along the twist axis but it does not explain the constant Si−Si distance in a different axis unless there is some distortion of the Si−O distances. So, for example, if there was a twisting along an Si−O1−Si linkage (see Figure 4) the Si−O1−Si distance would stay constant but the Si−O4−Si distance would change (provided the Si−O4 distance did not change). Whichever the mechanism it has to be reconciled with the fact that the Si−Si distances are nearly the same at low and high temperatures.

To be able to obtain more details about the structural changes of chabazite with temperature we needed structural models whose calculated PDFs agreed with the experimentally obtained PDFs. We used as our first structural models the structures reported by Woodcock et al. of chabazite at 293 and 873 K.[4] The PDFs of these structures were calculated and the profile parameters refined to compare them to the experimental PDFs (Figure 5). Since our experimental PDFs were obtained at different temperatures we are expecting some differences in the structures. The structures may vary significantly between 753 and 873 K but they should be nearly identical between 293 and 308 K. For the profile refinement of the reported structures we used the lattice parameters calculated at the experimental temperatures using the equations and parameters described by Woodcock et al.[4] Comparison of the PDFs at low temperature shows good agreement between the structure reported by Woodcock et al.[4] and our data. However, the peak splitting in the experimental PDF at around 3.8 Å is not well described by

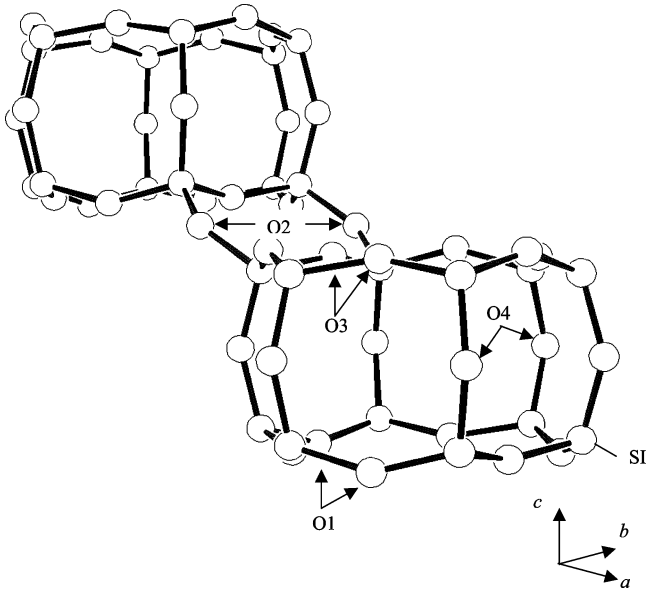


**Figure 4.** View of a double six membered ring (D6R) of chabazite down the [010] axis. Each ring is made up of alternating Si−O1−Si−O3 bonds connected to the other ring via Si−O4−Si bonds. Each D6R then is connected to another D6R via Si−O3−Si−O2 bonds. The basis axes shown here are for the hexagonal setting.

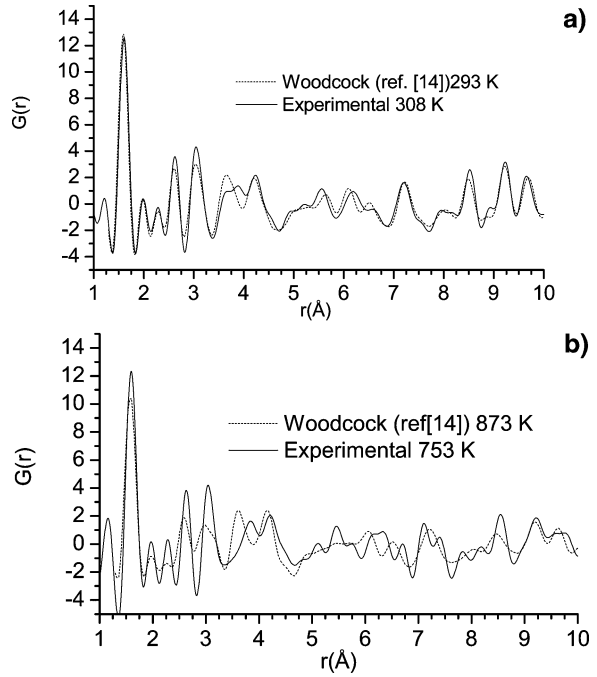


**Figure 5.** (a) Calculated PDF of Woodcock's structural model at 293 K[4] and experimental PDF at 308 K, $R_w = 0.2441$ (b) Calculated PDF of Woodcock's structural model at 873 K,[4] experimental PDF at 753 K, $R_w = 0.5191$. The profile parameters were refined in the calculated models for realistic comparison to the experimental results.

the structural model. These differences are significant because it is at these distances that we see the first major differences in the experimental PDFs at the two temperatures. We were not able to refine satisfactorily the profile parameters of the 873 K structure PDF as the positions of the peaks diverged greatly.

To obtain better structural models we optimized the published chabazite structures by minimizing the potential energy and the free energy at given temperatures using GULP. The structures obtained by the minimization of the potential energy of the 293 and 873 K structures reported[4] resulted in similar final structures, as might be expected because there is no kinetic energy contribution. On the other hand, the structures obtained by the minimization of the free energy at the two temperatures were significantly different.

**TABLE 1: Unit Cell Obtained by the Free Energy Minimization of the Si-Chabazite Structure at 308 and 753 K in Rhombohedral Setting[a]**

| | 308 K | | | 753 K | | |
|---|---|---|---|---|---|---|
| | *x* | *y* | *z* | *x* | *y* | *z* |
| Si | 0.3338 | 0.8785 | 0.107 | 0.3342 | 0.878 | 0.1072 |
| O1 | 0.253 | 0.8974 | 0.253 | 0.2531 | 0.8982 | 0.2531 |
| O2 | 0.5 | 0.1497 | 0.8503 | 0.5 | 0.1497 | 0.8503 |
| O3 | 0.3251 | 0.0259 | 0.0259 | 0.327 | 0.0259 | 0.0259 |
| O4 | 0.2579 | −0.2579 | 0 | 0.2584 | −0.2584 | 0 |

[a] Unit cell parameters: 308 K, a = 9.2283 Å, α = 94.7858°; 753 K, a = 9.1878 Å, α = 94.6928°. Space group $R\bar{3}m$ (No. 166).

The free energy minimization can be done with and without the zsisa approximation. However, results from optimizations done without the approximation were erroneous as is evident from the deformation of the lattice parameters of the resulting structures. This agrees with the findings of Gale that in materials where there are low-frequency modes due to rotation of polyhedra, like in zeolites, or molecular fragments, complete free energy minimization with GULP is not reliable except at very low temperatures. Free energy minimization with the zsisa was able to predict a decrease in volume with temperature in Si-chabazite from 2331.6 Å$^3$ at 308 K to 2309.53 Å$^3$ at 753 K, a decrease of 0.94%. The atomic positions are listed in Tables 1 and 2. Using the equation for coefficient of linear expansion

$$\alpha = \frac{1}{l_0}\frac{\Delta l}{\Delta T} \tag{5}$$

the α predicted is $-9.11 \times 10^{-6}$ K$^{-1}$ for the $a = b$ axis and $-3.1 \times 10^{-6}$ K$^{-1}$ for the $c$ axis, which is within the range found by Woodcock et al.[4]

The crystalline structures obtained by the free energy minimization with GULP describe much better the behavior of the PDF data in comparison to the structures obtained by Woodcock et al.[4] The structure optimized at 308 K predicts the splitting of the Si−O peak between 3.65 Å and 3.9 Å although not quantitatively (Figure 6 shows the experimental and calculated PDFs). The 753 K optimized structure was also a much better fit to the high-temperature experimental PDF than the published structure at 873 K. The fact that the zsisa approximation was suitable for obtaining a structure that agreed better with experiments supports our earlier observation that the structural changes with temperature were rather subtle. The agreement, however, was only semiquantitative as the model differs from experiment in the critical area between 3.3 and 3.9 Å and some of the rest of the peaks are not well described both in position and in intensity. We attempted difference modeling[14] in which instead of modeling the individual PDFs we modeled the difference between the two experimental PDFs. However, the structural differences of chabazite at the two temperatures were significant enough for this method to be unreliable.

We went further and optimized the free energy of chabazite at a range of temperatures from 300 to 900 K in 50 deg steps to determine if there was any other structure that could fit our experimental PDFs better but we found that the predicted structures were very similar so there was no significant improvement on the fits on either of the experimental PDFs. This is due to the zsisa under which it is mainly the lattice parameters and not the atomic positions that are changed with temperature with the optimization; so a change in atomic

**TABLE 2: Structural Changes of the Structures of Chabazite with Temperature as Obtained by the Different Methods**

| | Woodcock | | | Optimized | | | average RMC | | |
|---|---|---|---|---|---|---|---|---|---|
| | 293 K | 873 K | diff | 308 K | 753 K | diff | 308 K | 753 K | diff |
| ⟨Si−O1⟩ | 1.60 | 1.64 | 0.04 | 1.60 | 1.59 | 0.00 | 1.60 | 1.63 | 0.03 |
| ⟨Si−O2⟩ | 1.62 | 1.64 | 0.03 | 1.60 | 1.59 | −0.01 | 1.59 | 1.58 | −0.02 |
| ⟨Si−O3⟩ | 1.59 | 1.57 | −0.02 | 1.61 | 1.61 | 0.00 | 1.59 | 1.59 | 0.00 |
| ⟨Si−O4⟩ | 1.58 | 1.52 | −0.06 | 1.61 | 1.60 | 0.00 | 1.62 | 1.58 | −0.04 |
| **⟨Si−O⟩** | **1.60** | **1.59** | **0.00** | **1.60** | **1.60** | **0.00** | **1.60** | **1.59** | **0.00** |
| ⟨Si−O1−Si⟩ | 149.80 | 143.83 | −5.97 | 149.30 | 149.11 | −0.19 | 150.62 | 145.99 | −4.63 |
| ⟨Si−O2−Si⟩ | 148.38 | 146.81 | −1.56 | 144.94 | 145.22 | 0.28 | 148.04 | 149.76 | 1.72 |
| ⟨Si−O3−Si⟩ | 147.21 | 144.14 | −3.07 | 148.99 | 149.14 | 0.15 | 155.84 | 147.38 | −8.46 |
| ⟨Si−O4−Si⟩ | 148.02 | 144.40 | −3.63 | 150.37 | 150.43 | 0.06 | 143.31 | 147.64 | 4.33 |
| **⟨Si−O−Si⟩** | **148.35** | **144.80** | **−3.56** | **148.40** | **148.48** | **0.08** | **149.45** | **147.69** | **−1.76** |
| ⟨Si−O1−Si⟩ | 3.09 | 3.13 | 0.04 | 3.08 | 3.07 | −0.01 | 3.10 | 3.12 | 0.02 |
| ⟨Si−O2−Si⟩ | 3.11 | 3.15 | 0.04 | 3.05 | 3.03 | −0.02 | 3.06 | 3.04 | −0.02 |
| ⟨Si−O3−Si⟩ | 3.05 | 2.99 | −0.06 | 3.10 | 3.10 | 0.00 | 3.10 | 3.05 | −0.05 |
| ⟨Si−O4−Si⟩ | 3.04 | 2.89 | −0.14 | 3.11 | 3.10 | 0.00 | 3.07 | 3.04 | −0.03 |
| **⟨Si−O−Si⟩** | **3.07** | **3.04** | **−0.03** | **3.09** | **3.08** | **−0.01** | **3.08** | **3.06** | **−0.02** |

positions needs to occur. We used the structures optimized at the respective temperatures of the experiments and did a full refinement of the structures. This, however, did not improve significantly the fits of the structures as they were at a local minimum solution that PDFfit could not change.

Taking advantage of the reasonably good fit of the optimized structure and experimental PDF at low temperature we looked into the structure to determine what structural changes might be occurring with the temperature increase. The most obvious change is that the peak at 3.67 Å disappears giving rise to a higher intensity both at higher (3.86 Å) and lower distances. The low-temperature peak at 3.67 Å corresponds in the optimized structure to the Si−O4 third neighbor distance but there is also another peak in our model at 3.54 Å corresponding to the Si−O3 third neighbor distance. The changes in the PDF then suggest that the structural change involves a change in the Si−O4 and Si−O3 third neighbor distance.

Since the initial attempts did not yield a structure that agreed with our high-temperature PDF we used the Reverse Monte Carlo (RMC) technique combined with the real-space Rietveld to fit the data. For these refinements we used one rhombohedral unit cell repeated infinitely in 3D. This method was successful in finding a model that described quantitatively the experimental PDFs (Figure 7). Due to the nature of the RMC technique the resulting structures were disordered by including different possible configurations of the atoms, in this way accounting for the diffuse information in the experimental scattering data.

RMC refinements were also made using the hexagonal setting of the structure, which effectively is three unit cells of chabazite in the rhombohedral setting. However, the resulting structures tended to have very long Si−O bond lengths, greater than the absolute maximum expected of 1.84 Å (according to the experimental PDFs). This was due to the increased freedom of movement by having more available atoms to move and the presence of the termination ripples in the experimental PDFs. We, thus, decided that using the rhombohedral unit cell was the best approach as the initial optimized structure was already a reasonably good fit to the experimental PDFs so the atoms

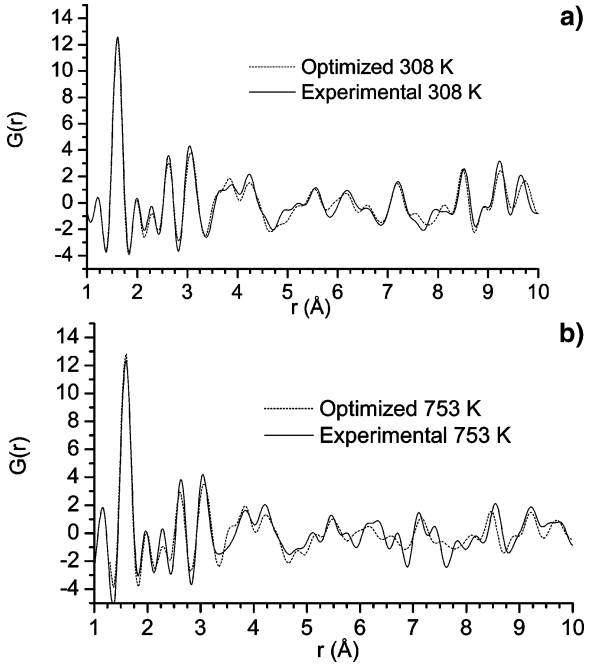


**Figure 6.** Experimental and calculated PDF of the models optimized by free energy minimization at (a) 308 K, $R_w = 0.2116$, and (b) 753 K, $R_w = 0.3115$. The profile parameters of the calculated PDFs were refined for better comparison.

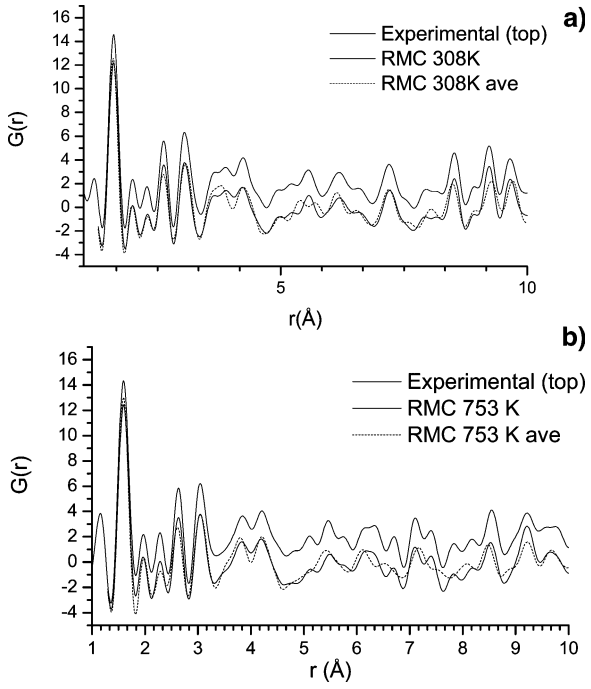


**Figure 7.** (a) Experimental and calculated PDFs of the models obtained by Reverse Monte Carlo in combination with real-space Rietveld and their average crystalline structure: (a) 308 K, $R_w = 0.1182$, 0.2416, and (b) 753 K, $R_w = 0.1711$, 0.2999. The experimental PDFs have been shifted two units up for clarity.

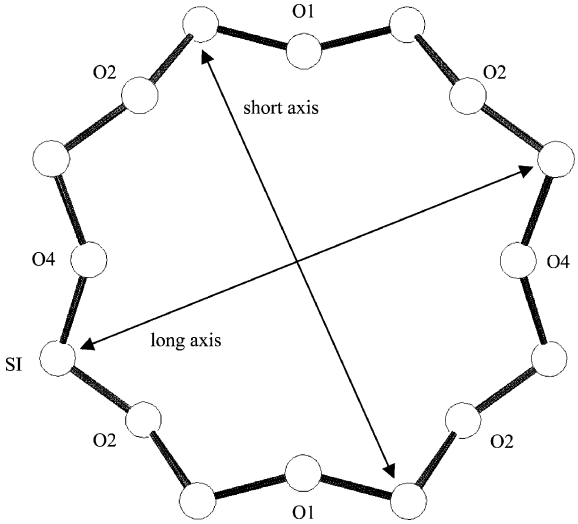


**Figure 8.** Change in the shape of the chabazite ellipsoidal 8MR windows.

did not need an increased freedom of movement and because when the final RMC structures were averaged they were actually a better fit to the experimental PDFs than the optimized structures, which was ultimately our goal.

As expected the general Si−O and Si−Si average distances and distributions remain nearly the same with temperature while the O−O average distance increases slightly. However, what was found by the RMC method was that there is a change in the dimensions of the Si−O and Si−O−Si linkages of the tetrahedra with temperature, as was found by Woodcock et al.[4] *and* in contrast to the optimized structures (see Table 2). The average Si−O1 next neighbor distance was found to increase with temperature, the Si−O3 stays approximately constant, and the Si−O2 and Si−O4 average next neighbor distances decrease. The Si−O1−Si and Si−O3−Si average angles decrease by more than 4°, the average Si−O2−Si angle increases slightly, and Si−O4−Si increases by more than 4°, as shown Table 2. The overall effect is that all the Si−O*x*−Si average distances decrease except the Si−O1−Si distance. Since the Si−O4−Si linkages are along the *c* axes of the hexagonal cell a shortening of the Si−O4−Si distance explains the contraction of the *c* axis with temperature and the net contraction of the Si−O3−Si and Si−O1−Si distances explain the contraction of the *a* and *b* axes. The contraction of the Si−O2−Si distance affects all axes. One interesting observation from these structural models is that the ellipsoidal 8MR windows of chabazite are becoming less ellipsoidal with temperature. The Si−Si distance along the long axis of the 8MR ellipsoidal window decreases from 7.988 Å to 7.947 Å and the short axis increases from 7.747 Å to 7.764 Å (in the average RMC structures) giving a net pore volume decrease (Figure 8). This may have implications in the shape selective absorption capacity of chabazite with temperature.

The structural changes described above are true to both the disordered RMC structure and the average crystalline structure derived from it although the actual values are different. Table 3 shows the atomic positions of the atoms of these average structures and Figure 7 includes their PDFs. It is clear from Figure 7 that the RMC average structures do not agree to the same extent with the experimental PDFs as the disordered structures. This is due to the fact that the limited number of atoms in the average structure is not sufficient to describe the disorder information contained in the experimental PDF. This is most evident in the change in the PDFs between 3.4 Å and 4.06 Å that in our RMC structures corresponds to a larger range

**TABLE 3: Average Unit Cell Obtained by the RMC of the Si-Chabazite Structure at 308 K in Rhombohedral Setting[a]**

| | 308 K | | | 753 K | | |
|---|---|---|---|---|---|---|
| | *x* | *y* | *z* | *x* | *y* | *z* |
| Si | 0.3332 | 0.8769 | 0.1054 | 0.3334 | 0.8768 | 0.1028 |
| O1 | 0.2514 | 0.8907 | 0.2514 | 0.2549 | 0.8983 | 0.2549 |
| O2 | 0.5 | 0.1465 | 0.8535 | 0.5 | 0.1434 | 0.8566 |
| O3 | 0.3173 | 0.0136 | 0.0136 | 0.3325 | 0.0256 | 0.0256 |
| O4 | 0.2656 | −0.2656 | 0 | 0.2609 | −0.2609 | 0 |

[a] Unit cell parameters: 308 K, $a = 9.2283$ Å, $\alpha = 94.7858°$; 753 K, $a = 9.1978$ Å, $\alpha = 94.6928°$. Space group $R\bar{3}m$ (No. 166). The actual average values of the *x* of O2 and the *z* of O4 were 0.5012 and 0.5015 and −0.0085 and 0.0197 at 308 and 753 K, respectively, and they were set to 0.5 and 0 to keep the symmetry of the unit cell.

in the third neighbor Si−O3 and Si−O4 distances that the average RMC unit cell cannot describe.

It is difficult to extract a mechanism of contraction from this Reverse Monte Carlo model because of the disordered nature of the final structures. However, these results suggest that besides internal vibrations distorting the tetrahedra there is a strong mode that travels along the Si−O3−Si−O4−Si−O3−Si linkages inside the D6R that does not move to other D6R as the Si−O2−Si linkages linking two D6R's do not appear to change significantly with temperature. Here we are assuming that it is a dynamic mode what is causing the static changes in the chabazite structure described above.

## Conclusions

We have gained new insight into the mechanism of contraction of zeolite chabazite with temperature using the PDF method. Our main results were obtained from analysis of the differences in the experimental PDFs with temperatures and by comparison to optimized structures. We have shown the advantages of the PDF method on these types of problems and also how to use interatomic potentials and the Reverse Monte Carlo technique to obtain improved models for the local structures of zeolites with temperature. We conclude that as the temperature increases the tetrahedra actually distort, thus the mechanism of contraction does not necessarily involve rigid rocking of the tetrahedra.

By comparison of the Reverse Monte Carlo optimized structures at low and high temperatures we conclude that the main differences in the structures involved Si−O4 and Si−O3 third neighbor distances suggesting that in addition to the internal vibrations of the tetrahedra there is a mode at high temperatures that travels along the Si−O4−Si−O3−Si of a D6R without moving through the Si−O2−Si linkage to another D6R. This would explain why the experimental PDFs only differ in discrete regions. It is because of the dynamical origin of the information included in the pair distribution function at high temperature that a small static unit cell cannot describe it quantitatively. One possible way to sort this out is to find a pair distribution functions using only the elastic scattering information, or information from the Bragg peaks, and compare it to this pair distribution function that includes diffuse scattering; the difference describes the dynamical information.

**Acknowledgment.** We thank Robyn J. Accardi for the synthesis and $^{29}$Si MAS NMR spectra of chabazite. We would also like to thank Sarvjit Shastri at APS and Valeri Petkov for their help obtaining and reducing the X-ray data. Funding of this work was partially provided by the National Science Foundation under Grant No. CTS-0085036. Use of the Advanced Photon Source was supported by the U.S. Department

of Energy, Basic Energy Sciences, Office of Science, under Contract No. W-31-109-Eng-38.

## References and Notes

(1) Woodcock, D. A.; Lightfoot, P.; Wright, P. A.; Villaescusa, L. A.; Diaz-Cabanas, M. J.; Camblor, M. A. *J. Mater. Chem.* **1999**, *9*, 349.

(2) Park, S. H.; Kunstleve, R. W. G.; Graetsch, H.; Gies, H. The thermal expansion of the zeolites MFI, AFI, DOH, DDR, and MTN in their calcined and as synthesized forms. In *Prog. Zeolite Microporous Mater., Part A-C* **1997**, *105*, 1989.

(3) Lightfoot, P.; Woodcock, D. A.; Maple, M. J.; Villaescusa, L. A.; Wright, P. A. *J. Mater. Chem.* **2001**, *11*, 212.

(4) Woodcock, D. A.; Lightfoot, P.; Villaescusa, L. A.; Diaz-Cabanas, M. J.; Camblor, M. A.; Engberg, D. *Chem. Mater.* **1999**, *11*, 2508.

(5) Attfield, M. P.; Sleight, A. W. *Chem. Mater.* **1998**, *10*, 2013.

(6) Hammonds, K. D.; Heine, V.; Dove, M. T. *J. Phys. Chem. B* **1998**, *102*, 1759.

(7) Hammonds, K. D.; Dove, M. T.; Giddy, A. P.; Heine, V. *Am. Mineral.* **1994**, *79*, 1207.

(8) Tao, J. Z.; Sleight, A. W. *J. Solid State Chem.* **2003**, *173*, 442.

(9) Baur, W. H. *J. Solid State Chem.* **1992**, *97*, 243.

(10) Evans, J. S. O. *J. Chem. Soc., Dalton Trans.* **1999**, 3317.

(11) Martinez-Inesta, M.; Peral, I.; Proffen, T.; Lobo, R. *Microporous Mesoporous Mater.* **2005**, *77*, 55.

(12) *Local Structure from Diffraction*; Billinge, S. J. L., Thorpe, M. F., Eds.; Plenum Press: New York, 1998; p 137.

(13) Billinge, S. J. L.; Kanatzidis, M. G. *Chem. Commun.* **2004**, 749.

(14) Egami, T.; Billinge, S. J. L. *Underneath the Bragg Peaks*: *Structural Analysis of Complex Materials*; Pergamon: New York, 2003; Vol. 7.

(15) Tschaufeser, P.; Parker, S. C. *J. Phys. Chem.* **1995**, *99*, 10609.

(16) Gale, J. D. *J. Phys. Chem. B* **1998**, *102*, 5423.

(17) Couves, J. W.; Jones, R. H.; Parker, S. C.; Tschaufeser, P.; Catlow, C. R. A. *J. Phys. Condens. Matter* **1993**, *5*, L329.

(18) Gale, J. D. *J. Chem. Soc., Faraday Trans.* **1997**, *93*, 629.

(19) Diaz-Cabanas, M. J.; Barrett, P. A.; Camblor, M. A. *Chem. Commun.* **1998**, 1881.

(20) Warren, B. E. *X-ray Diffraction*; Dover Publications: Mineola, NY, 1990.

(21) Klug, H. P.; Alexander, L. E. *Diffraction Studies of Noncrystalline Materials*; John Wiley & Sons:New York, 1954.

(22) Jeong, I. K.; Thompson, J.; Proffen, T.; Turner, A. M. P.; Billinge, S. J. L. *J. Appl. Crystallogr.* **2001**, *34*, 536.

(23) Jeong, I. K.; Heffner, R. H.; Graf, M. J.; Billinge, S. J. L. *Phys. Rev. B* **2003**, *67*.

(24) Proffen, T.; Billinge, S. J. L. *J. Appl. Crystallogr.* **1999**, *32*, 572.